World Scientific
www.worldscientific.com

CONCEPTUAL DESIGN OF A SUPERCONDUCTING QUADRUPOLE WITH ELLIPTICAL ACCEPTANCE AND TUNABLE HIGHER ORDER MULTIPOLES

SHASHIKANT MANIKONDA* and JERRY NOLEN†

Physics Division, Argonne National Laboratory,
9700 South Cass Avenue, Argonne, IL 60439, USA
*manikonda@anl.gov
†nolen@anl.gov

MARTIN BERZ‡ and KYOKO MAKINO§

Department of Physics and Astronomy, Michigan State University,
East Lansing, MI 48824, USA
‡berz@msu.edu
§makino@msu.edu

For charged particle beams that are wider in the dispersive plane compared to the transverse plane it is cost efficient to utilize magnets that accept beams with elliptic cross section. In this paper we presents the conceptual design of a quadrupole magnet with elliptic cross section and with tunable higher order multipoles. The design consists of 18 superconducting race-track coils placed on two hollow concentric rhombic prism support structures.

To compute the magnetic field for the proposed design a new method of calculating 2D and 3D fields for the air core magnets based on differential algebra (DA) techniques is developed. We will present the new method and discuss its implementation of new numerical tools based on this method in the code COSY Infinity.

Keywords: Differential algebra; magnet design; beam physics.

PACS numbers: 29.30.Aj, 29.30.Ep, 41.85.-p

1. Introduction

Next-generation radioactive beam facilities like the proposed AEBL[1,2] facility in US and the newly constructed BIGRips[3] facility in Japan, require the use of large aperture superconducting multipole magnets. Since the charged particle beams used in such facilities are wider in the dispersive plane than the transverse plane it is cost efficient to utilize magnets with elliptic cross sections. Such elliptic cross section design usually leads to generation of high order multipoles. In this paper we present a new design for a quadrupole magnet with an elliptic cross-section and with tunable higher order multipoles. The analysis of this design requires the

development of new numerical tools to compute the multipole expansion of the magnetic field starting from the Biot-Savart law and Ampere's law. The Differential Algebra (DA) techniques have been utilized to extract such multipole expansions for the air-core magnets.

In sections 2 and 3 we will present the background and discuss the theory and implementation of the new computational tools using the differential algebra (DA) techniques. In section 4 we present the details of the design of the new quadrupole magnet with tunable high order multipoles. We will discuss both the 2D and 3D design and also discuss the practicle range of multipole field strengths that can be achieved with this design.

2. Differential Algebra Techniques and Field Computations

In beam physics the DA techniques have traditionally been used for the computation of the high-order Taylor expansion of the transfer maps and design and analysis of accelerator lattices.[4,5,6,7] In recent years the DA techniques have been applied to solve DAEs, ODEs and PDEs.[8,9,10,11,12] For these applications the DA is used to develop techniques and algorithms to use a truncated Taylor expansion of a function on a computer. The numerical techniques based on DA have the unique advantage of getting high accuracy at a very small cost of the execution time and the computational resources compared to traditional techniques.

In the context of magnet design the DA techniques have so far been utilized to obtain magnetic fields from the analytic model of the magnet, consisting of line wire currents, obtained from codes like ROXIE.[13] The details of the method and it implementation are described in [14, 15]. The present work starts directly from the geometric model of the magnet and computes the multipole expansion of the fields. The method described in this paper is useful for both designing the magnets as well as multipole extraction of the fields, which can then be combined with the existing DA based transfer map computation tools. Hence, all the aspects from design of the magnet, extraction of transfer maps and finally its use in beam optic design and optimization can be performed in the same code.

3. Magnetic Field Due to Arbitrary Current Distribution

The Biot-Savart law and Ampere's law can be utilized to compute the magnetic field for an arbitrary current distribution. Usually, numerical integration is required to find the total magnetic field at any point. Below we describe a new scheme to perform such numerical integration using DA techniques.

For an arbitrary current distribution the proposed method discretizes the current domain and expresses the integral over the current domain as the sum of integrals over smaller intervals. For the line, surface or volume distribution we express the intervals in terms of one, two or three parameters and scale them such that the new interval is a box $[-1, 1]^n$, where $n \in 1, 2, 3$. We then Taylor expand the kernel appearing in the Biot-Savart law and the Ampere law in terms of the

observation point, $\vec{r}$, and previously defined parameters. Finally, we integrate in parameters over the interval $[-1, 1]^n$ and then sum over all the intervals to get the multipole expansion of the magnetic field about the observation point $\vec{r}$.

We now discuss the above scheme for computing the magnetic field by using the example of the current in a straight wire with a finite rectangular cross section. This particular case is of practical importance and we will use this to develop tools to design new accelerator magnets. These tools will later be used to analyse the proposed design of the quadrupole magnet in the section 4.

3.1. *Magnetic field computation for a wire with a rectangular cross section using DA*

For the case of a rectangular box of length l, width w and breath b, let the cross section be described by the unit vectors $\hat{n}_w$ along the width, and $\hat{n}_b$ along the breath. The unit vector $\hat{n}_l = \hat{n}_w \times \hat{n}_b$ then defines the cross section plane and is along the direction of the length of the rectangular box. The central axis can be described by $\vec{V}_c = \vec{V}_{c_0} + \lambda_3 \hat{n}_l$, where the vector $\vec{V}_{c_0}$ is the center of a face on the rectangular box that is perpendicular to the unit vector $\hat{n}_l$, and $\lambda_3 \in [0, l]$. Any point inside the box is given by

$$\vec{V}_p^{box}(\lambda_1, \lambda_2, \lambda_3) = \vec{V}_{c_0} + \frac{1}{2}(\lambda_1 b \hat{n}_w + \lambda_2 w \hat{n}_b) + \lambda_3 \hat{n}_l, \tag{1}$$

where the parameters $\lambda_1, \lambda_2 \in [-1, 1]$. The parameters $(\lambda_1, \lambda_2, \lambda_3)$ then completely describe a rectangular box. The equation (1) will be used in the next two sections to express the Biot-Savart law and Ampere's law in the DA framework.

3.1.1. *Magnetic field of a wire with a rectangular cross section using the Biot-Savart law and DA*

We can choose the direction of the current flow in the wire to coincide with the unit vector $\hat{n}_l$ and the magnitude to be I_0. Using the Biot-Savart law, we can write the magnetic field at an observation point $\vec{r}$ as

$$\vec{B}(\vec{r}) = \frac{\mu_0}{4\pi} \frac{I_0}{bw} \int_{-1}^{1} \int_{-1}^{1} \left[\int_0^l \frac{\left(\hat{n}_l \times \left(\vec{r} - \vec{V}_p^{box} \right) \right)}{\left| \vec{r} - \vec{V}_p^{box} \right|^2} d\lambda_3 \right] d\lambda_2 d\lambda_1, \tag{2}$$

where μ_0 is the permeability of vacuum. In SI units, the value is exactly expressed by $\mu_0 = 4\pi \times 10^{-7} N A^{-2}$. To perform integration with respect to λ_3 in the equation (2), we first split the domain of integration into smaller intervals. Let the length l be divided into N parts of the size $h = l / N$. Then the parameter λ_3 can be written as

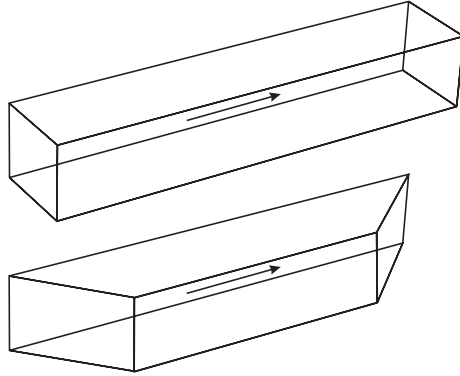$$\lambda_3(i) = \left(i + \frac{1}{2} v \right) h,$$

Fig. 1.   The schematic digram of a finite length current wire with rectangular cross section and (a) straight ending (b) inclined ending.

where $i = 0.5, \ldots, (N - 0.5)$, and $v \in [-1, 1]$. The position of a point inside the box in terms of the new parameters $(\lambda_1, \lambda_2, v)$ is given by

$$\vec{V}_p^{box}(i, \lambda_1, \lambda_2, v) = \vec{V}_{c_0} + ih\hat{n}_l + \frac{1}{2}(\lambda_1 b\hat{n}_1 + \lambda_2 w\hat{n}_2 + vh\hat{n}_l). \qquad (3)$$

The equation (2) can now be written as

$$\vec{B}(\vec{r}) = \frac{\mu_0}{4\pi} \frac{I_0}{bw} \sum_{i=0.5}^{i=N-0.5} \int_{-1}^{1} \int_{-1}^{1} \int_{-1}^{1} \frac{\left(\hat{n}_l \times \left(\vec{r} - \vec{V}_p^{box}(i)\right)\right)}{\left|\vec{r} - \vec{V}_p^{box}(i)\right|^2} \frac{l}{N} dv d\lambda_2 d\lambda_1. \qquad (4)$$

The parameters $(\lambda_1, \lambda_2, v)$ and the position $\vec{r}(x, y, x)$ become the DA variables with respect to which the kernel of the integral in the equation (4) is expanded to a high order. In the DA framework it is straightforward to perform the volume integral over the resulting polynomial representation.

In the DA frame work it is also straightforward to treat the wires with rectangular cross sections that have curved endings rather than the straight endings that are perpendicular to the direction of the current flow. Let the two surfaces at the start and the end of the wire carrying the current be expressed as $\lambda_3 = g(\lambda_1, \lambda_2)$ and $\lambda_3 = f(\lambda_1, \lambda_2)$. We can use the equation (4) to find the magnetic field due to this new configuration by noting

$$h(\lambda_1, \lambda_2) = \frac{f(\lambda_1, \lambda_2) - g(\lambda_1, \lambda_2)}{N},$$

where the step h is now a function of the parameters (λ_1, λ_2). The equation (3) can be modified to express a point inside the rectangular box with curved endings as

$$\vec{V}_p^{box}(i, \lambda_1, \lambda_2, v) \qquad = \vec{V}_{c_0} + (g(\lambda_1, \lambda_2) + i \cdot h(\lambda_1, \lambda_2)) \cdot \hat{n}_l \qquad (5)$$

$$+ 0.5 \cdot (\lambda_1 b \cdot \hat{n}_1 + \lambda_2 w \cdot \hat{n}_2 + v \cdot h(\lambda_1, \lambda_2) \cdot \hat{n}_l). \qquad (6)$$

When the surfaces are just inclined planes, the functions f and g are just linear combinations of the parameters λ_1 and λ_2. The Figure 1 shows the schematic diagram of a wire with straight ending and inclined ending. The inclined ending case is useful in the implementation of the numerical tool to compute the magnetic field due to a current carrying coil with a rectangular cross section.

3.1.2. *Magnetic field of an infinitely long wire with a rectangular cross section using Ampere's law and DA*

Once again, we can choose the direction of the current in the infinitely long wire with a rectangular cross section to coincide with the unit vector $\hat{n}_l$ along the length of the wire. Let the vector $\vec{V}_p$ defined by

$$\vec{V}_p = \vec{V}_c + \frac{1}{2}\left(\lambda_1 b \hat{n}_b + \lambda_2 w \hat{n}_w\right), \tag{7}$$

describes a point inside a rectangle cross section with breath b and width w and centered at a point $\vec{V}_c$. The closest distance $r_\perp$ between the observation point $\vec{r}$ and the line passing through the point $\vec{V}_p$ and in the direction $\hat{n}_l$ is given by

$$r_\perp = \left|\left(\vec{r} - \vec{V}_p\right) - \left(\hat{n}_l \cdot \left(\vec{r} - \vec{V}_p\right)\right)\hat{n}_l\right|,$$

where $\vec{V}_p$ is given by the equation (7). Ampere's law can then be written as

$$\vec{B}\left(\vec{r}\right) = \int_{-1}^{1}\int_{-1}^{1}\frac{\mu_0}{2\pi}\frac{I_0}{b \cdot w}\frac{\left(\hat{n}_l \times \frac{\left(\vec{r} - \vec{V}_p\right)}{|\left(\vec{r} - \vec{V}_p\right)|}\right)}{r_\perp}d\lambda_1 \cdot d\lambda_2. \tag{8}$$

The equation (8) can be used to compute the magnetic field of an infinitely long wire with a rectangular cross section. The parameters (λ_1, λ_2) become the DA variables with respect to which the kernel of the integral in the equation (8) is expanded to high order, and DA integration is performed over the resulting polynomial representation.

3.1.3. *COSY INFINITY tools for magnetic field computations*

Due to their frequent use in the magnet design, a dedicated set of tools has been written for the rectangular cross section wire and coil in the code COSY INFINITY.[16,17] These tools use the differential algebraic framework available in COSY to Taylor expand, integrate and evaluate the kernels appearing in the equations(8) and (4).

For 2D design, a tool to compute the field for an infinitely long wire with a rectangular cross section has been implemented. For 3D design, a tool to compute the magnetic field of a finite length wire of a rectangular cross section has been implemented. A finite length wire can have the current entrance and exit planes inclined to the central axis or the direction of the current flow. By combining four such current wires, as shown in Figure 2, a separate tool to compute the magnetic

field of a current coil of a rectangular cross section has also been implemented. The wires have current entrance and exit planes tilted by 45° in opposite directions.

Using orders around 10, accuracy of about 14 digits can be achieved using these tools. In addition to providing highly accurate results in the form of the local Taylor expansion of the magnetic field, the DA based implementation has a unique advantage of easily obtaining the curl and divergence of the magnetic field at any given point. This offers one way to quickly verify if the magnetic field satisfies Maxwell's equations.

4. The Conceptual Design of an Asymmetric-Aperture Quadrupole Magnet with Adjustable Multipole Components

For charged particle beams that are wider in the dispersive plane than the transverse plane it is cost efficient to utilize magnets that accept beams with elliptic cross sections . In this section we present the conceptual design of a quadrupole magnet with an elliptic cross section and with tunable high order multipoles. The design consists of 18 superconducting racetrack coils placed on two hollow concentric rhombic prism support structures. It would require 28 racetrack coils to create the same number adjustable multipoles with circular aperture magnets (quadrupole through decapole).

A combination of superconducting racetrack coils is used to produce the desired magnetic field inside an elliptic cross section. By the proper choice of dimensions, current density, and placement of these coils, various combinations of the quadrupole field and the higher order multipole fields can be achieved. In this example, the support structure that holds these coils in place consists of two concentric hollow rhombic prisms, with the ratio of the diagonals of the rhombus is 2. The cross section view showing the arrangement of the current coils on the support structure is shown in Figure 3. The signs "+" and "−" indicate the direction of the current to produce a positive multipole term. The superconducting racetrack coils on the inner rhombic prism produce quadrupole and octupole fields. The racetrack
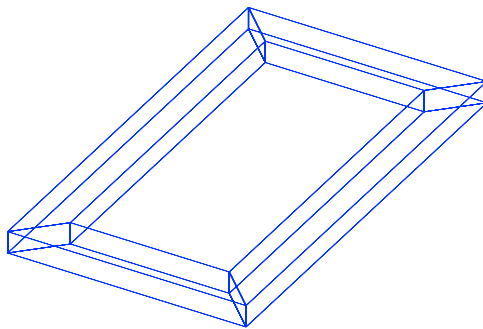

Fig. 2.   The schematic digram of a current coil.

Table 1. The center position of the current carrying coils in the first quadrant.

Coil Description	Position of Coils		Current
	x	y	
Inner Coils			
Quadrupole	0.4473	0.8222E-01	-QI1
Octupole	0.3473	0.1322	-QI2
Octupole	0.1973	0.2072	+QI2
Quadrupole	0.9736E-01	0.2572	+QI1
Outer Coils			
Hexapole	0.5591	0.1604	+HI1
Decapole	0.4591	0.2104	+HI2
Decapole	0.3091	0.2854	-HI2
Hexapole	0.2091	0.3354	-HI1
Dipole Corrector	0.8385E-01	0.4172	-HI3

coils on the outer rhombic prism produce hexapole and decapole fields, and also allow for a limited dipole field for correction purposes. The numerical example discussed here the coil cross section are arbitrarily chosen to be square with a peak current density of 100 A/mm^2. This analysis applies applies strictly to air core magnets. In practice an external iron shield would most likely be used and field analysis would be done numerically with a 3D numerical code such as ROXIE.

Due to symmetry in the design about the central axis, it is sufficient to describe only one quarter of the magnet. Figure 4 shows one quarter of the cross section. The positions and the direction of the coils in this quarter are specified in Table 1. All the coils have square cross section with thickness of 0.1 m.

In Table 1 the quantities $QI1, QI2, HI1, HI2, HI3$ are the magnitude of the currents. For any given configuration of the inner current coils, the currents $(QI1, QI2)$ can be used as parameters to obtain different quadrupole and octupole strength. Similarly, for any given configuration of the outer coils, the currents $(HI1, HI2)$ can be used as parameters to get the desired hexapole and decapole field strength.

From the construction point of view it is cost efficient if the same type of coils can be used. We use current coils of the same shape and size to generate the quadrupole and hexapole fields. Also, we use the same type of current coils for octupole and decapole fields. For an optimized final design these arbitrary constraints can be relaxed.

4.1. *2D design of the quadrupole magnet*

For a 2D design the magnet is considered to be infinitely long, thus avoiding any fringe field effects. This leads to purely transverse magnetic fields (2D fields). In this case a coil can be viewed as two current wires of infinite length and finite cross section which are separated by certain distance. The currents in these wires are equal in magnitude but are opposite in direction. We can use Ampere's law, given by equation (8), to compute the magnetic field of individual wires. The total magnetic field is then the superposition of the fields produced by these wires. Below we show the results for two special cases that produce pure quadrupole and hexapole fields.
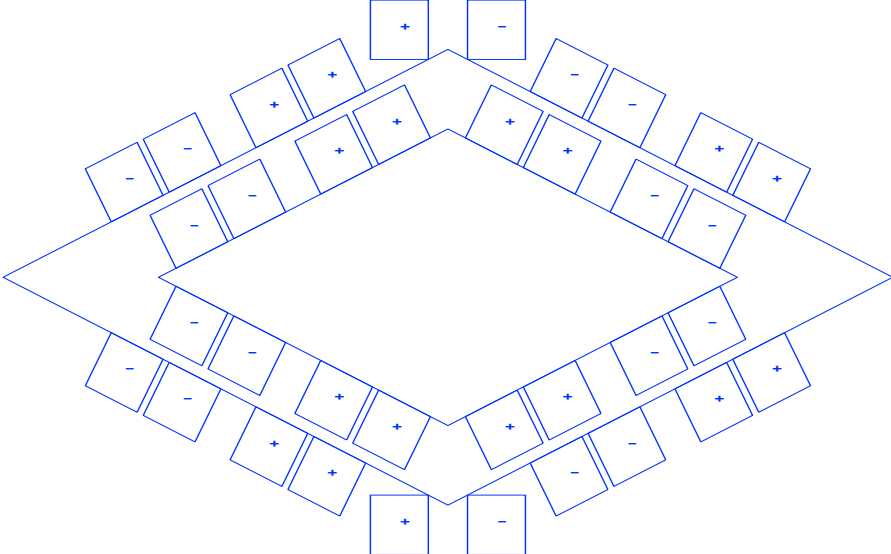
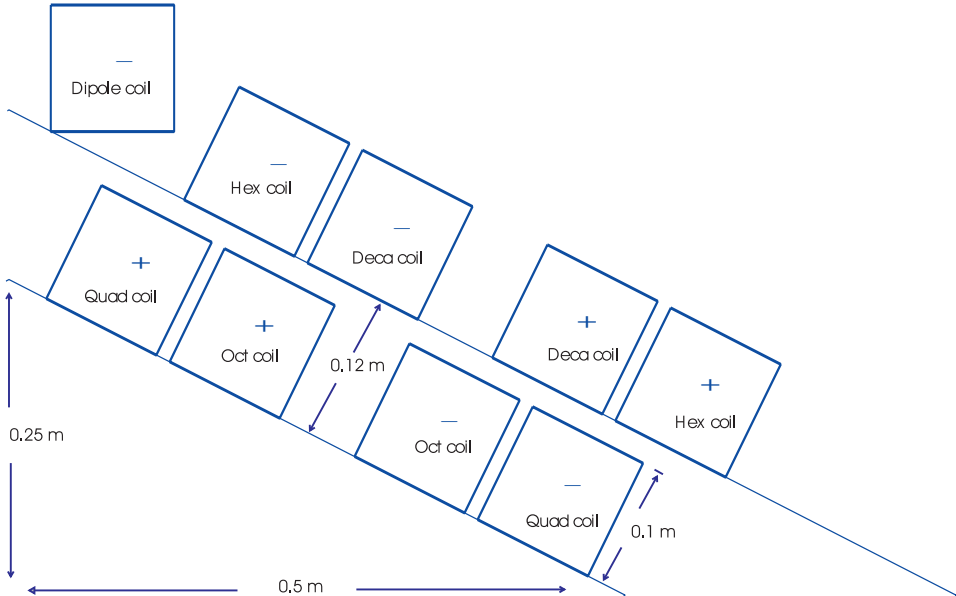Fig. 3.   The cross section view of the asymmetric-aperture multipole.

Fig. 4.   The layout of the racetrack coils in the first quadrant.

Table 2.   The amplitude of currents required for pure quadrupole and hexapole configurations.

Coil Description	Pure quadrupole configuration (million Amps)	Pure hexapole configuration (million Amps)
Inner Coils		
QI1	3.965	0
QI2	0.080	0
Outer Coils		
HI1	0	0.499
HI2	0	0.938
HI3	0	0.448

Current configuration required to generate a pure quadrupole component and hexapole component are given in Table 2. The fifth order Taylor expansion of the magnetic field about the point $(0.0, 0.0, 0.0)$, for each of these configurations is given in Table 3 and Table 4. The entries in the first and second column provide the Taylor expansion of x and y components of the magnetic field. Each row provides coefficient in the expansion whose exponent is described in column three. In the notation for the exponent the give expansion order with respect to x and y.

Table 3.   The fifth order Taylor expansion of the magnetic field about the point (0.0,0.0,0.0) for the current configuration producing a pure quadrupole field.

```
        Bx                        By                   xy
   0.4440892098501E-15      0.000000000000          00
   0.000000000000          46.09565826333           10
  46.09565826333            0.000000000000           01
  -0.7105427357601E-14      0.000000000000           20
   0.1421085471520E-13     -0.1421085471520E-13      11
   0.000000000000           0.1136868377216E-12      21
   0.000000000000          -0.2842170943040E-13      12
   0.7815970093361E-12      0.000000000000           03
  -0.1421085471520E-13      0.000000000000           40
   0.000000000000           0.5684341886081E-13      31
  -0.2273736754432E-12     -0.1705302565824E-12      13
  -0.4263256414561E-13      0.5684341886081E-13      04
   0.000000000000         -3956.535097021            50
 -19782.67548511            0.000000000000           41
   0.000000000000         39565.35097021             32
 39565.35097021             0.000000000000           23
   0.000000000000        -19782.67548511             14
 -3956.535097021            0.000000000000           05
      -------------------------------------------------
```

Table 4.   The fifth order Taylor expansion of the magnetic field about the point (0.0,0.0,0.0) for the current configuration producing a pure hexapole field.

```
        Bx                    By               xy
    0.000000000000     -0.8604228440845E-15    00
   -0.4718447854657E-15 0.000000000000         10
    0.000000000000     -0.3885780586188E-15    01
    0.000000000000    -18.24792017395          20
  -36.49584034790       0.000000000000         11
    0.000000000000     18.24792017395          02
   -0.1776356839400E-14 0.000000000000         21
   -0.1776356839400E-14 0.2664535259100E-14    12
    0.2220446049250E-14 -0.4440892098501E-15   03
   -0.1776356839400E-14 -0.3463895836830E-13   40
   -0.2593480985524E-12 0.000000000000         31
    0.000000000000     0.4547473508865E-12     22
    0.1705302565824E-12 0.1953992523340E-13    13
    0.4440892098501E-14 -0.4174438572591E-13   04
    0.1776356839400E-14 0.8881784197001E-15    50
    0.1421085471520E-13 0.1421085471520E-13    41
    0.2842170943040E-13 0.3552713678801E-13    32
    0.2131628207280E-13 0.000000000000         23
   -0.5684341886081E-13 -0.7105427357601E-14   14
   -0.4440892098501E-14 -0.3552713678801E-14   05
   ---------------------------------------------
```

4.1.1. *Operational plots*

We now discuss the practical range of multipole field strength that can be achieved with this numerical example. We have mentioned that the currents $(QI1, QI2, HI1, HI2)$ can be used as parameters to get the desired quadrupole and higher order multipole strengths. However, there is a maximum limit on the current density that the superconducting coils can support. This puts a limit on the maximum quadrupole and other multipole field strength that can be achieved. Because of the fact that each multipole is achieved by superimposing the fields of several coils, this leads to operating diagrams showing achievable multipole settings.

   To study this situation in detail, we now look at how the multipole strength depends on the currents. The matrix given in the equation (9) relates the multipole field strength at the horizontal half aperture to the currents in the coils for the specific case of a horizontal half aperture of 0.5 m and a vertical half aperture of 0.25 m. In the notation $B^y_{(1111)}$, the superscript denotes the "y" component of the magnetic field and the subscript (1111) gives the exponent in transport notation. Thus, $B^y_{(1111)}$ is the coefficient of x^4 in the Taylor expansion of the "y" component

of the magnetic field, or the decapole term in the expansion. The equations (10) provide relationships between the coefficients of other multipole terms in the Taylor expansion of the field to the principle multipole coefficients $B^y_{(11)}$, $B^y_{(111)}$ and $B^y_{(1111)}$.

$$
\begin{bmatrix} B^y_0 \\ B^y_{(1)} \\ B^y_{(11)} \\ B^y_{(111)} \\ B^y_{(1111)} \\ B^y_{(11111)} \end{bmatrix} = \begin{bmatrix} 0 & 0 & -0.25137 & -0.04316 & +0.37029 \\ +5.76974 & +2.40063 & 0 & 0 & 0 \\ 0 & 0 & -3.89914 & -2.08907 & -1.45431 \\ -0.40613 & +15.44685 & 0 & 0 & 0 \\ 0 & 0 & +1.66569 & -2.32478 & +2.99743 \\ -31.32418 & -12.0759 & 0 & 0 & 0 \end{bmatrix} \cdot \begin{bmatrix} QI1 \\ QI2 \\ HI1 \\ HI2 \\ HI3 \end{bmatrix}
\tag{9}
$$

$$
\begin{aligned}
B^y_{(22)} &= -B^y_{(11)} \\
B^y_{(122)} &= -3B^y_{(111)} \\
-\frac{B^y_{(1122)}}{6} &= B^y_{(2222)} = B^y_{(1111)} \\
B^x_{(2)} &= B^y_{(1)} \\
B^x_{(12)} &= 2B^y_{(11)} \\
\frac{B^x_{(112)}}{3} &= -B^x_{(222)} = B^y_{(111)} \\
B^x_{(1112)} &= -B^x_{(1222)} = 4B^y_{(1111)}
\end{aligned}
\tag{10}
$$

It can be seen from the coefficient of the two quadrupole coils (QI1 and QI2), given in the equation 9, that the inner pair (QI2) produces mainly an octupole term, whereas the outer pair (QI1) produces dominantly a quadrupole term. Then coefficients can be tuned in an optimized design by variation of the zero order coil geometry parameters.

4.1.2. *Operational plot for the quadrupole and the octupole fields*

From the equation (9) it can be seen that the quadrupole field strength and the octupole field strength are coupled via the currents ($QI1, QI2$). We vary both of these current densities in the range $[-10^8, 10^8]$ A/m^2 and plot the resulting octupole field strength and the quadrupole field strength; the results are shown in Figure 5. This plot gives the possible values of the quadrupole and octupole strength that can be achieved with the configuration of the coils described in the section 4.

4.1.3. *Operational plot for the hexapole and decapole fields*

From the equation (9) it can also be seen that the dipole, hexapole and decapole field strength are coupled via the currents ($HI1, HI2, HI3$). However, under normal
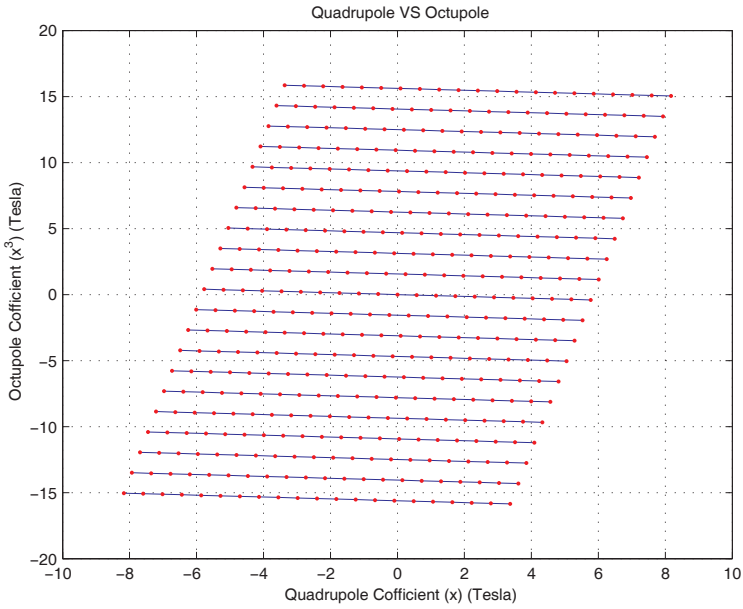
Fig. 5.   The operational plot for the quadrupole and the octupole. The coefficients are computed at the horizontal half aperture.
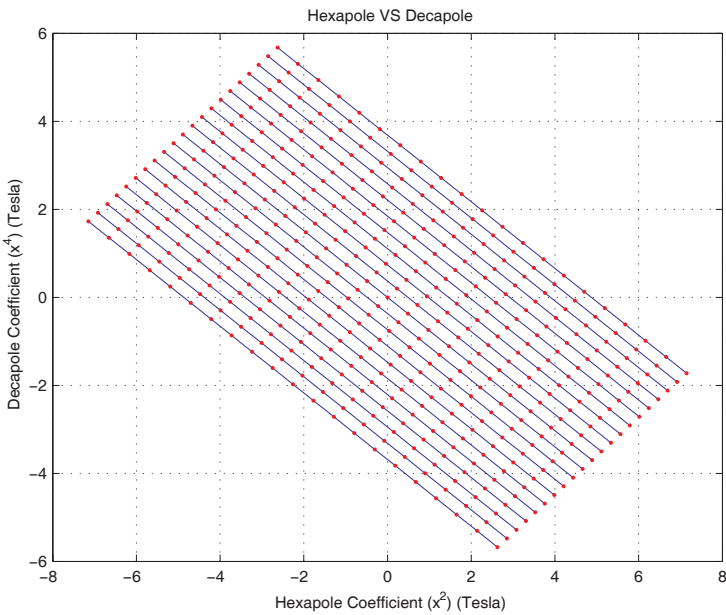

Fig. 6.   The operational plot for the hexapole and the decapole. The coefficients are computed at the horizontal half aperture.

operation, we have a strict requirement of zero dipole field for this magnet. The dipole field is set zero by the proper choice of the current $HI3$. Once again we vary the current densities of all currents in the range $\left[-10^8, 10^8\right]$ A/m^2 and plot the decapole field strength versus the hexapole field strength; the results are shown in Figure 6. This plot gives the possible values of the hexapole and decapole strength that can be achieved with the configuration of the coils described in the section 4.

4.1.4. *Optimization of the operational region*

As mentioned above the details of terms in the matrix given in the equation (9) are influenced by the geometrical design parameters of the system. In order to optimize the operational region of the currents and the fields, we need to find the optimal geometric configuration of the coils described in the section 4, where the optimal design is defined as the one that would decouple the influence of the octupole coil current on the quadrupole component of the field and vice versa. And, at the same time maximize the coupling strength of the current in quadrupole coils on the quadrupole component of the field, and maximize the coupling strength of the current in octupole coils on the octupole component of the field. The same type of optimization is also required for the hexapole and decapole components of the field. Alternatively, for a specific optical system the zero order parameters can be chosen to emphasize operation in a necessary region of the 2D operating diagram. For example, this example is more effective in the upper right quadrant of Figure 5 than in the upper left quadrant.
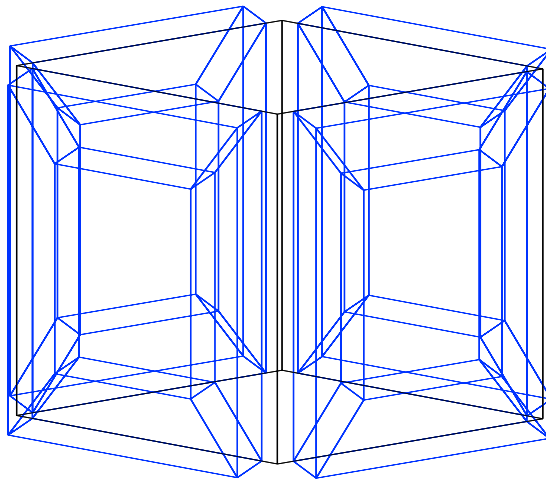

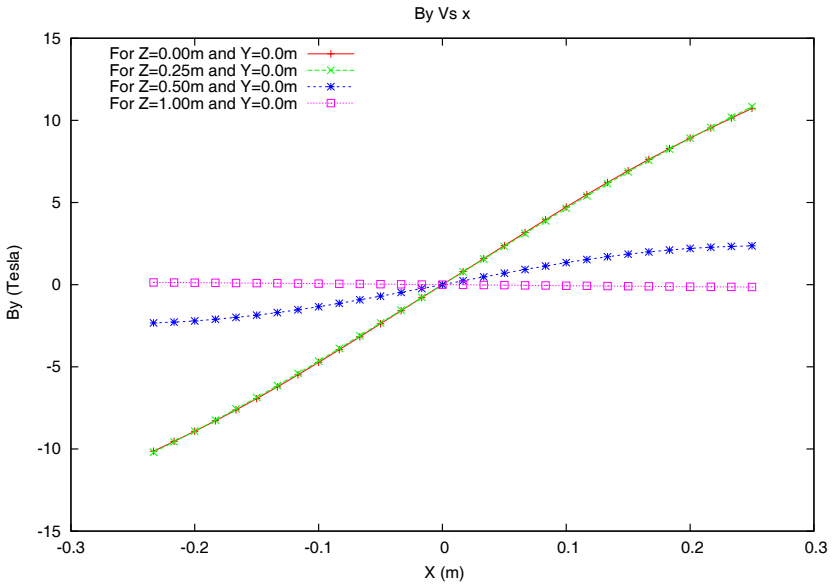Fig. 7.   The three dimensional layout of quadrupole coils.

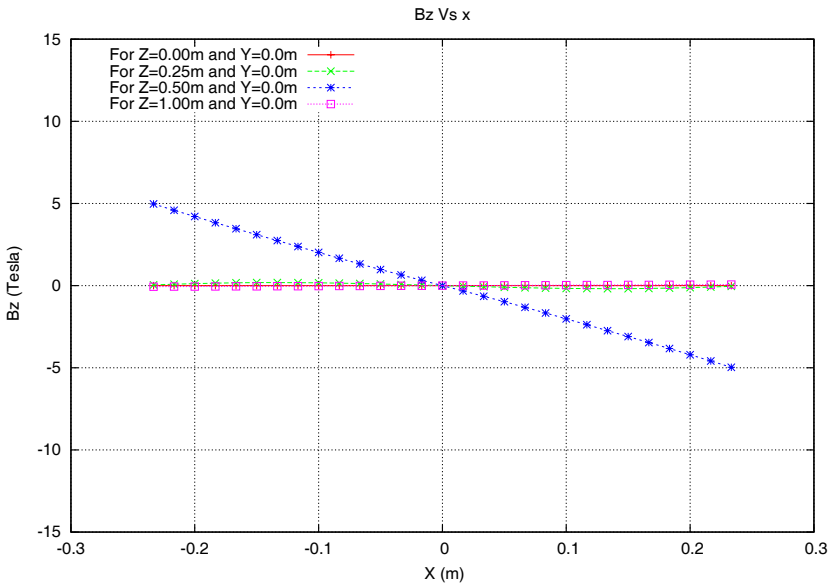Fig. 8.   The plot for B_y vs x on four planes.

Fig. 9.   The plot for B_z vs x on four planes.
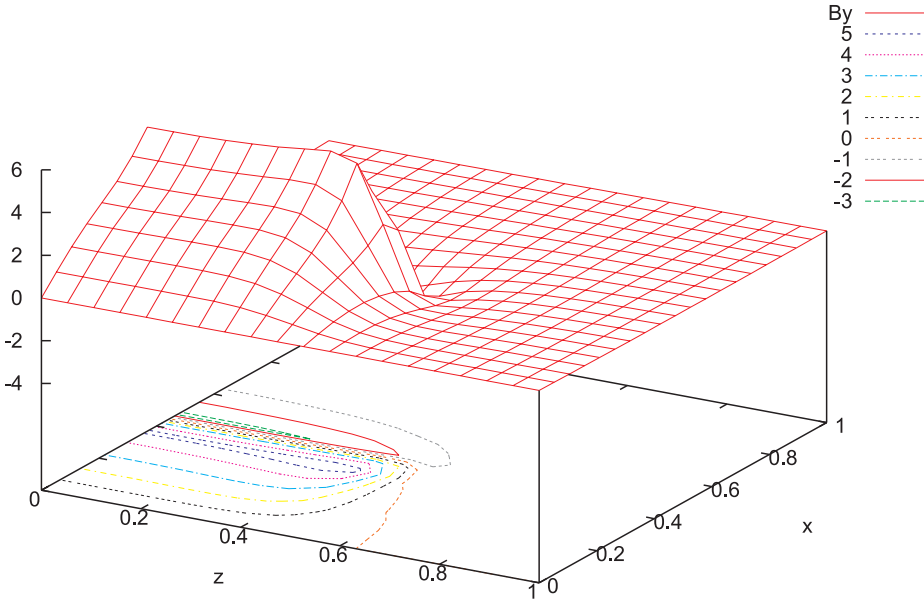
By for Quadrupole at Y=0 plane

Fig. 10. The plot of Y component of magnetic field on the midplane, $y = 0\ m$. Only the magnetic field in the first quadrant is shown.

4.2. *3D design of the quadrupole and the fringe field analysis*

We consider a magnet of length $1\ m$, extending from $-0.5\ m \leq z \leq 0.5\ m$, and cross-section described by the design presented in the section 4.1. The 3D layout of the quadrupole with four current coils is shown in Figure 7. We compute the magnetic field generated by this coil configuration on four different planes, perpendicular to the central axis, located at the center $z = 0\ m$, quarter length $z = 0.25\ m$, the entrance of the magnet $z = 0.5\ m$ and out side the magnet $z = 1.0\ m$. The DA based tool to compute field for rectangular cross-section coils, described in section 3.1.3, is used to compute multipole expansion of the field. Figures 9 shows the x, y, z components of the magnetic field on these planes. Note that since the length of the magnet is large compared to the aperture of the magnet, the magnetic field in x, y at the center of the magnet is nearly identical to the magnetic field obtained by the 2D design in the section 4.1. In the z direction the magnitude of the magnetic field is of the order $\sim 10^{-16}$, which is zero for all practical purposes. As we start going away from the center, we observe deviation from the ideal behavior $(z = 0)$. We see that at $z = 0.25\ m$ there is no significant deviation from ideal behavior in the x and y components of the magnetic field. In the z direction we notice that the magnetic field is nonzero. However, the magnitude is still small compared to the components B_x and B_y. At the entrance of the magnet we see that the magnetic

By for the Quadrupole at X=0.25m and Y=0.05m
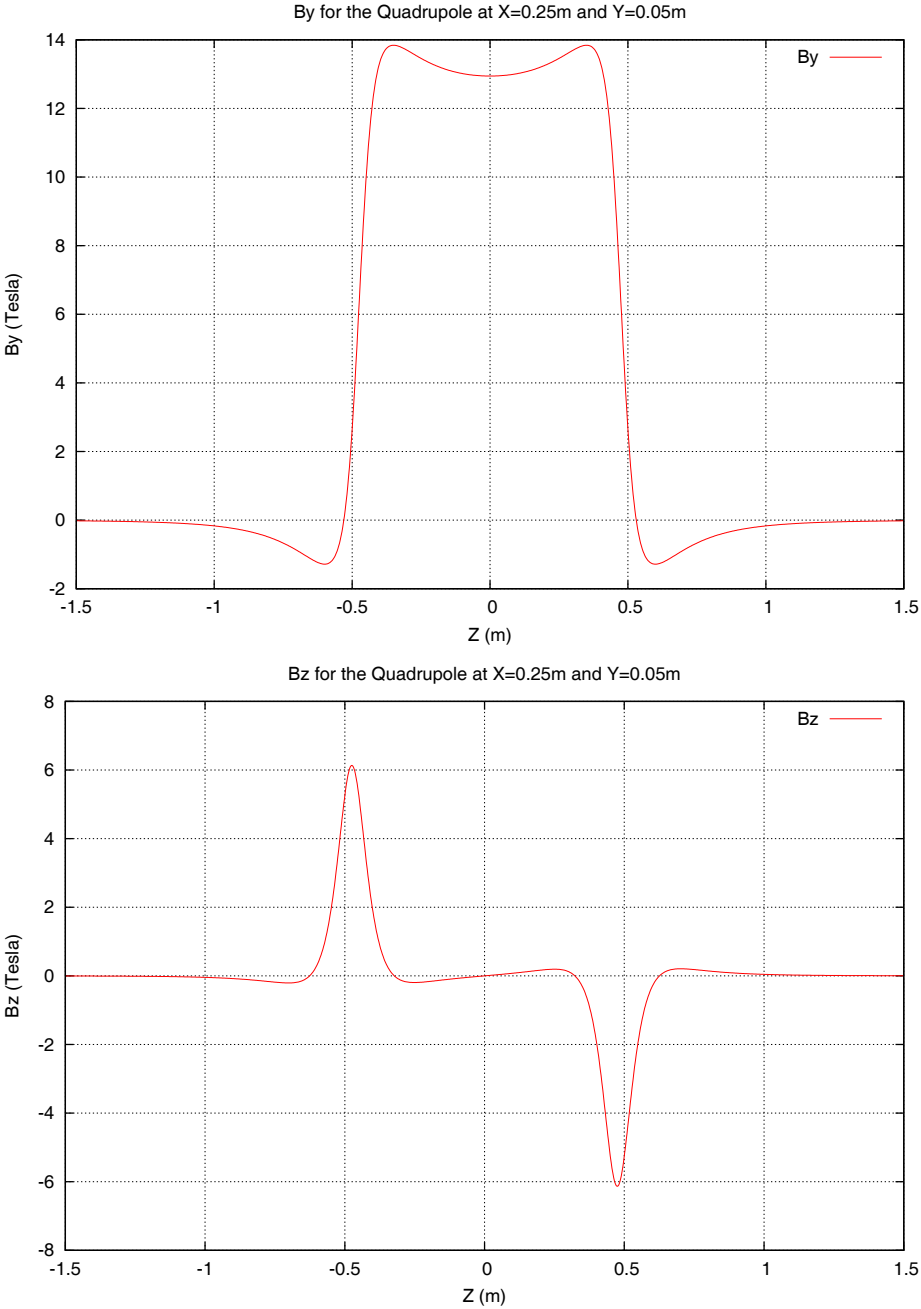
Bz for the Quadrupole at X=0.25m and Y=0.05m

Fig. 11.   Upper plot shows the y component and the lower plot shows the z component of magnetic field along the length of the magnet.

field in x, y falls by a factor of five. But the z component is almost three times as large as the field in x or y. On a plane 0.5 m away from the entrance of the magnet the overall field falls off significantly and its magnitude is $\sim 10^{-1}$ *tesla*.

The figure 10 shows the y-component of the magnetic field on the first quadrant of the magnet on the $y = 0$ m plane. The region stretches from the center of the magnet to $0.5m$ (half length of the magnet) outside the magnet in both x and z directions. Here the fringe field fall off in the region can be clearly seen. Finally, in figure 11 we show the plot of y and z component of the magnetic field along the length of the magnet.

5. Summary

A new concept for a superconducting quadrupole with elliptic acceptance and tunable high order multipoles is presented. The DA techniques have been utilized to design and optimize the magnet in a simple and efficient way. The DA based techniques have the advantage of providing the complete multipole decomposition of the field. From the detailed 3D analysis it is possible to construct the high order transfer map for the magnet. And thus provide means to perform the integrated simulations of both the design and optimization of accelerator magnets and also the beam optics using such magnets in the same code.

Acknowledgments

References

1. J.A. Nolen. Plans for an Advanced Exotic Beam facility in the U.S. In *Proceedings of the Ninth International Conference on Nucleus-Nucleus Collisions -(NN2006)*, volume 787, pages 84–93, 2007.
2. J.A. Nolen. Overview of the u.s. rare isotope accelerator proposal. *Nuclear Physics A*, 734:661–668, 2004.
3. Toshiyuki Kubo. In-flight ri beam separator bigrips at riken and elsewhere in japan. In *14th International Conference on Electromagnetic Isotope Separators and Techniques Related to their Applications*, volume 204, pages 97–113, 2003.
4. M. Berz. Differential algebraic description of beam dynamics to very high orders. *Particle Accelerators*, 24:109, 1989.
5. M. Berz. Differential algebra - a new tool. Technical Report LBL-27033, Lawrence Berkeley Laboratory, Berkeley, CA, 1989.
6. M. Berz. High-order description of accelerators using differential algebra and first applications to the SSC. In *Proceedings, Snowmass Summer Meeting*, Snowmass, Co, 1988.
7. M. Berz. Differential algebra - a new tool. In *Proceedings of the 1989 IEEE Particle Accelerator Conference*, page 1419. IEEE, 1989.
8. S. L. Manikonda and M. Berz. Multipole expansion solution of the Laplace equation using surface data. *Nuclear Instruments and Methods*, 258:175–183, 2006.

9. K. Makino. *Rigorous Analysis of Nonlinear Motion in Particle Accelerators*. PhD thesis, Michigan State University, East Lansing, Michigan, USA, 1998. Also MSUCL-1093.

10. J. Hoefkens. *Verified Methods for Differential Algebraic Equations*. PhD thesis, Michigan State University, East Lansing, Michigan, USA, 2001.

11. J. Hoefkens, M. Berz, and K. Makino. Efficient high-order methods for ODEs and DAEs. In G. Corliss, C. Faure, A. Griewank, L. Hascoët, and U. Naumann, editors, *Automatic Differentiation of Algorithms from Simulation to Optimization*, pages 343–348. Springer, 2002.

12. Y. F. Chang and G. F. Corliss. ATOMFT: Solving ODEs and DAEs using Taylor series. *Computers and Mathematics with Applications*, 28:209–233, 1994. see also http://www.mscs.mu.edu/ georgec/Pubs/journ.html#1994a.

13. S. Russenschuck. A computer program for the design of superconducting accelerator magnets. Technical Report CERN AT/95-39, CERN, 1995.

14. B. Erdélyi. *Symplectic Approximation of Hamiltonian Flows and Accurate Simulation of Fringe Field Effects*. PhD thesis, Michigan State University, East Lansing, Michigan, USA, 2001.

15. G. Sabbi. Magnetic field analysis of HGQ coil ends. Technical Report TD-97-040, Fermilab, 1997.

16. M. Berz and K. Makino. COSY INFINITY beam physics manual. Technical Report MSUHEP-60804, Department of Physics and Astronomy, Michigan State University, East Lansing, MI 48824, 2006. see also http://cosy.pa.msu.edu.

17. M. Berz and K. Makino. COSY INFINITY programmer's manual. Technical Report MSUHEP-60803, Department of Physics and Astronomy, Michigan State University, East Lansing, MI 48824, 2006. see also http://cosy.pa.msu.edu.

18. Manikonda Shashikant. *High order finite element methods to compute Taylor transfer maps*. PhD thesis, Michigan State University, East Lansing, Michigan, USA, 2006.